ROYAL SOCIETY
OF CHEMISTRY

COMMUNICATION
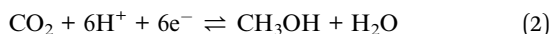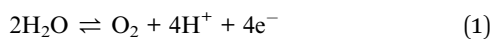
Cooperative electrochemical water oxidation by Zr nodes and Ni–porphyrin linkers of a PCN-224 MOF thin film†

P. M. Usov,‡ S. R. Ahrenholtz,‡ W. A. Maza, B. Stratakes, C. C. Epley, M. C. Kessinger, J. Zhu and A. J. Morris*

Here, we demonstrate a new strategy for cooperative catalysis and proton abstraction *via* the incorporation of independent species competent in the desired reactivity into a metal–organic framework (MOF) thin film. The highly porous MOF, designated as PCN-224-Ni, is constructed by Zr–oxo nodes and nickel(II) porphyrin linkers. Films of PCN-224-Ni were grown *in situ* on FTO and were found to electrochemically facilitate the water oxidation reaction at near neutral pH.

Increasing energy demands and steadily accumulating levels of detrimental greenhouse gases necessitates the continued search for alternative, renewable energy sources.[1] Solar energy has the capacity to power all of human civilization and therefore, has emerged as a leading carbon-neutral energy alternative.[2] However, two challenges remain in the harnessing of solar energy: (1) the intermittent nature of the sun necessitates energy storage technology, and (2) the cost of efficient solar cell installations provides a barrier to widespread adoption. Artificial photosynthesis – the direct conversion of sunlight into a stored fuel – is one possible method by which to overcome the first barrier. At the simplest level, an artificial photosynthetic system must (1) absorb light, generating an excited state; (2) separate charge, resulting in long-lived redox equivalents, and (3) catalyze desired reactivity. The reactivity catalyzed is the oxidation of water and the reduction of either CO_2 or protons to yield a combustible fuel, eqn (1)–(4).

$$2H_2O \rightleftharpoons O_2 + 4H^+ + 4e^- \tag{1}$$

$$CO_2 + 6H^+ + 6e^- \rightleftharpoons CH_3OH + H_2O \tag{2}$$

$$CO_2 + 8H^+ + 8e^- \rightleftharpoons CH_4 + 2H_2O \tag{3}$$

$$2H^+ + 2e^- \rightleftharpoons H_2 \tag{4}$$

Department of Chemistry, Virginia Tech, Blacksburg, VA 24061, USA. E-mail: ajmorris@vt.edu; Tel: +1 540 231 5585

† Electronic supplementary information (ESI) available. See DOI: 10.1039/c6ta05877a

‡ Indicates co-first author.

Akin to natural photosynthesis, a current thrust in catalyst development is to build proton management capabilities about the periphery of the catalytically active site. Indeed, proton management has been used to produce impressive enhancements in catalytic activity across all aspects of artificial photosynthesis – proton reduction,[3] CO_2 reduction,[4–6] and water oxidation.[7] The aforementioned reactions are proton-coupled electron transfer processes (PCET) with three possible reaction pathways to traverse: (1) proton transfer followed by electron transfer (PTET), (2) electron transfer followed by proton transfer (ETPT), or concerted PCET. Manipulation of the proton transfer pathway *via* the secondary coordination sphere directly affects kinetic and thermodynamic barriers. Therefore, at the simplest level, reaction rates can increase if proton-transfer is rate limiting. Alternatively, the balance between the barriers of PTET, ETPT, and PCET could shift such that the overall reaction mechanism is altered. Herein, we report an alternative to traditional catalyst approaches, metal–organic frameworks (MOFs), which provide a new paradigm for how to manipulate proton management and catalytic activity in heterogeneous electrocatalysis.

The properties and ease of design offered by MOFs presents a unique alternative to common water oxidation catalysts. MOFs are porous, 3D coordination polymers commonly comprised of metal–oxo clusters bridged by organic linker molecules.[8] In this regard, MOFs bridge the gap between molecular and material based approaches to water oxidation. The pore size and environment, surface area, and morphology of MOFs can be synthetically tuned to generate ideal properties for a variety of applications. The porosity imparted by the size and geometry of the linkers, as well as the coordination sphere around the metal clusters affords MOFs an increased surface area and a higher density of accessible catalytic sites as compared to traditional catalysts.[9,10]

In particular, MOFs containing porphyrinic macrocycles as linkers are attractive due to the reactive nature of these molecules.[11–14] Porphyrin-based moieties are ubiquitous in nature, capable of catalyzing a wide range of reactions.[15–18] However,

16818 | *J. Mater. Chem. A*, 2016, **4**, 16818–16823

This journal is © The Royal Society of Chemistry 2016

MOFs incorporating free-base and metallo-porphyrins are often limited by their structural stability in polar solvents, particularly water. Recently, this limitation has been addressed by the development of porphyrinic MOFs comprised of highly oxophilic metal ions, such as Zr^{4+} and Al^{3+} (*e.g.* PCN-222, 223, 224, 225, MOF-525, 545 and Al-PMOF), which provide considerable improvement in structural and chemical stabilities of the resulting frameworks.[19–26] Several of these porphyrinic MOFs have shown promise as electrocatalytic agents facilitating the reduction of CO_2.[18,27]

The chemical properties of metal clusters that comprise MOF structures also contribute to the overall framework reactivity. A high diversity of available metal ions and their synthetic tunability makes them attractive candidates as catalytic sites. In particular, Brønsted and Lewis acid/base properties of nodes, as well as coordinated guest molecules, such as water, have been previously utilized for the catalysis of a number of organic transformations.[28] Furthermore, additional reactive sites can be generated within the framework by doping with different metal ions[29] or through introduction of missing linker defects at the metal node.[30] Overall, there is a considerable potential for engineering framework nodes and combining their properties with the organic linkers in order to achieve novel cooperative behavior.

In this report a porphyrin-containing MOF, PCN-224-M (PCN = porous coordination network, M = Ni^{2+}) constructed with nickel(II) *meso*-tetrakis(4-carboxyphenyl) porphyrin, Ni(II)TCPP, linkers is presented as an active water oxidation promoter. PCN-224-Ni is a Zr(IV)-based MOF in which the octahedral $Zr_6(\mu_3-O)_4(\mu_3-OH)_4(OH)_6(OH_2)_6(COO^-)_6$ secondary building units (SBUs) are connected by six Ni(II)TCPP ligands, forming two open channels with node-to-node diameters of 23.7 and 15.1 Å, respectively, and a pore diameter of ~19 Å (Fig. 1A and S1†).[20] The open structure and large pores afford PCN-224-Ni a BET surface area of 2600 m^2 g^{-1}, one of the largest amongst porphyrinic MOFs, and a total pore volume of 1.59 cm^3 g^{-1} as calculated from N_2 adsorption isotherms.[20] These features allow for rapid diffusion of H_2O, O_2, and electrolyte throughout the framework. Due to the large surface area and pore volume of PCN-224-Ni, the high density of catalytic sites per area could be easily accessible by water molecules, which would result in considerably improved catalytic efficiency compared to non-porous heterogeneous catalysts. For example, in a film one unit cell thick, PCN-224-Ni has a density of *ca.* 8×10^{13} catalytic sites cm^{-2}, approximately 3 times greater than a monolayer of Ni(II)TCPP.

While there have been three reports of MOFs as water oxidation catalysts, the work reported herein demonstrates the first example of cooperative chemistry driven by the combination of an active, catalytic linker and proton-accepting node in a MOF thin film formed *in situ*.[31–33] The PCN-224-Ni thin films have been prepared by a solvothermal reaction on fluorine-doped tin oxide (FTO) conductive substrates. The heterogeneous MOF catalyst is active towards the oxidation of water at near neutral pH with Faradaic efficiencies consistent with that of the Ni(II)TCPP in solution. PCN-224-Ni films produced significantly more oxygen compared to films prepared with the
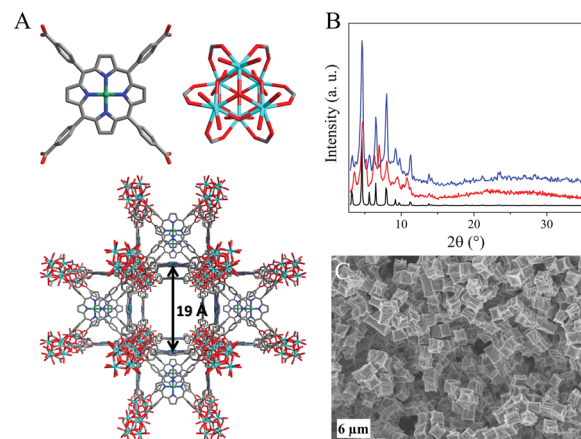

Fig. 1 (A) Ni(II)TCPP linker and the $Zr_6(\mu_3-O)_4(\mu_3-OH)_4(OH)_6(OH_2)_6(COO^-)_6$ secondary building unit of PCN-224-Ni (top) and PCN-224 structure with the Ni(II)-to-Ni(II) distance illustrated (bottom).[20] Hydrogen atoms have been omitted for clarity. Carbon: gray; oxygen, red; nitrogen, blue; nickel, green; zirconium, light blue. (B) PXRD pattern of simulated PCN-224-Ni from single crystal data[20] (black), synthesized PCN-224-fb (red), and PCN-224-Ni (blue) powders; (C) SEM of PCN-224-Ni film.

non-metallated (or free-base) H_2TCPP ligand, designated as PCN-224-fb. Films were prepared *via* incubation of a FTO substrate in a solvothermal reaction containing $ZrCl_4$ and Ni(II) TCPP (for PCN-224-Ni) or H_2TCPP (for PCN-224-fb) in the presence of formic acid as a modulator. Powder X-ray diffraction (PXRD) was used to confirm the structure of the MOF powder, which was consistent with the PCN-224 topology (Fig. 1B).[20] SEM imaging of the films shows crystallite features consistent with the cubic PCN-224 unit cell with a film thickness of *ca.* 30 μm (Fig. 1C, S2 and S3†). The film appears as a collection of particles mechanically immobilized on the FTO substrate. It is also possible that a self-assembled monolayer of Ni(II)TCPP has formed on the surface of FTO during the synthesis which would provide stronger interactions with the MOF particles.

The catalytic activity of PCN-224-Ni for water oxidation was investigated using electrochemical techniques. Cyclic voltammetric analysis of PCN-224-Ni under aqueous conditions revealed a rapid increase in current at 1.0 V *vs.* NHE (Fig. 2A, blue). The PCN-224-Ni current was significantly larger in magnitude compared to FTO (Fig. 2A, black) and the non-metallated
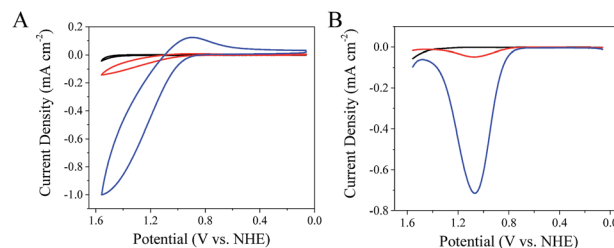

Fig. 2 (A) Cyclic voltammetry at 100 mV s^{-1} and (B) square wave voltammetry of FTO (black), PCN-224-fb (red), and PCN-224-Ni (blue) in aqueous 0.1 M $NaClO_4$.

PCN-224-fb film (Fig. 2A, red) and consistent with catalytic behavior. Square-wave voltammetry (SWV) of the films (Fig. 2B, blue and S4†) reveals an underlying broad electrochemical signature at 1.05 V *vs.* NHE attributed to the formation of a porphyrin cation radical species $[Ni^{II}TCPP]^{+\bullet}$, which is in thermal equilibrium with $[Ni^{III}TCPP]^{+}$. This process is overlapped with a second electrochemical event attributed to formation of the dication radical $[Ni^{III}TCPP]^{2+\bullet}$.[34,35] The oxidation of the porphyrin macrocycle to generate the initial radical species was also observed with PCN-224-fb films (Fig. 2B, red).[36,37]

The dependence of pH on the PCN-224-Ni water oxidation mechanism was determined by taking steady-state current measurements at constant potential in aqueous electrolyte (0.1 M NaClO$_4$). The pH of the solution was adjusted using 0.1 M HClO$_4$ and 0.1 M NaOH. PCN-224-Ni was found to demonstrate no dependence on proton concentration (Fig. S5†). This behavior is attributed to the fact that the redox-activity of the metalloligand is dominated by the $[Ni^{II}TCPP]^{0/+\bullet}$ process, which was reported to be pH independent for an analogous compound in solution.[35] The current–voltage (Tafel) behavior of PCN-224-Ni was investigated over a 200 mV overpotential range in 50 mV increments (Fig. S6†). From the onset of linearity in the Tafel plot, the overpotential for the water oxidation reaction was determined to be 450 mV. The Tafel slope obtained from the linear portion was 150 mV per decade with a corresponding exchange current density (j_o) of 7.7×10^{-10} A cm^{-2}, which are similar to other heterogeneous water oxidation catalysts.[38–42] The Tafel slope is indicative of an EC catalytic mechanism, consistent with electrochemical oxidation of the porphyrin macrocycle and Ni(II) metal centers followed by a chemical step.[43,44]

Under non-aqueous conditions (TBAPF$_6$/CH$_3$CN), the CVs of PCN-224-Ni exhibit a weak oxidation wave at 1.75 V *vs.* NHE, which appears as a shoulder on the background current (Fig. 3A) assigned to the $[Ni^{II}TCPP]^{0/+\bullet}$ process. The plot of log(j) *vs.* log(v) (where j = current density and v = scan rate) showed a linear trend with the slope of 0.6 (Fig. 3B). This relationship suggests diffusion limited electron transport through the film, which likely occurs by a charge hopping mechanism between the porphyrin moieties. A similar behavior has been observed previously for porphyrin-based MOF electrodes.[18,27,45] The water oxidation activity of PCN-224-Ni was supported by the increase in catalytic current with increasing water additions (Fig. 3C). The catalytic current density was found to increase linearly with $[H_2O]^{1/2}$, suggesting a first order reaction with respect to water (Fig. 3D and S7†).[46]

Controlled potential electrolysis (CPE) was performed on PCN-224-Ni in aqueous 0.1 M NaClO$_4$ at an applied potential of 1500 mV *vs.* NHE for 60 min. PCN-224-Ni maintained a higher current compared to bare FTO and PCN-224-fb films (Fig. 4A), as well as increased oxygen production (Fig. 4B). The fact that the Ni analogue generated significantly higher current than the free base MOF indicates that the Ni(II) center is critical to the observed electrocatalytic activity. Interestingly, the deposition of the free base PCN-224 on FTO resulted in lower current compared to the unmodified FTO electrode, which suggests that PCN-224-fb forms an insulating layer and inhibits the activity of
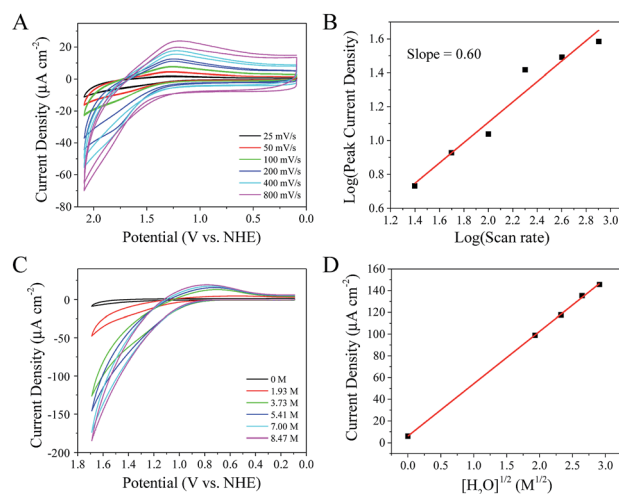

Fig. 3 (A) CV of PCN-224-Ni in 0.1 M TBAPF$_6$/CH$_3$CN as a function of scan rate; (B) a plot of the log(peak current density) *vs.* log(scan rate) gives a slope of 0.6, suggesting diffusion limiting electrochemical behavior; (C) CV of PCN-224-Ni in 0.1 M TBAPF$_6$/CH$_3$CN (black) with increasing H$_2$O concentrations; (D) plot of current density *vs.* $[H_2O]^{1/2}$ demonstrates a linear relationship.
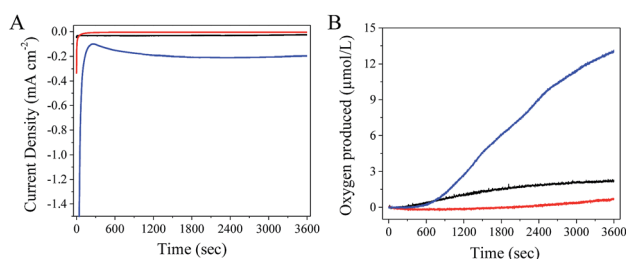

Fig. 4 (A) Controlled potential electrolysis (CPE) at 1500 mV *vs.* NHE in aqueous 0.1 M NaClO$_4$ and (B) oxygen evolved during CPE experiment of FTO (black), PCN-224-fb (red), and PCN-224-Ni (blue).

FTO. From this behavior it can also be concluded that the other components of the PCN-224 framework, such as Zr–oxo nodes, are inactive in the redox processes. The Faradaic efficiency of PCN-224-Ni was conserved with that of the Ni(II)TCPP ligand in solution under the same conditions (Fig. S8†). However, the efficiency was less than that of the similar water-soluble catalyst due to the mechanistic importance of phosphate buffer used in their study (*vide infra*).[35] The turnover frequency (TOF) of PCN-224-Ni was determined by digesting the MOF films in concentrated HNO$_3$ followed by ICP analysis for nickel content (Table S1†). The TOF was calculated under the assumption that all Ni centers of the film are catalytically active, which is an overestimation, and therefore, representative of the lower limit of TOF (eqn (5)). That said, the TOF for PCN-224-Ni was found to be $2\,(\pm 1) \times 10^{-4}$ s^{-1}.

$$TOF = \frac{mol\ O_2}{(mol\ Ni(II)TCPP) \times (electrolysis\ duration)} \quad (5)$$

Given Faradaic efficiencies <100% for O$_2$ production by PCN-224-Ni films, the alternative 2 electron reaction pathway

16820 | *J. Mater. Chem. A*, 2016, 4, 16818–16823

This journal is © The Royal Society of Chemistry 2016

resulting in H_2O_2 was considered. The immersion of indicator strips into the electrolyte at the end of electrolysis experiment did not detect any noticeable amount of H_2O_2, which means that its concentration in solution is below 0.5 mg L^{-1}. A similar lack of peroxide formation was reported by Han *et al.* for a water-soluble Ni(II) porphyrin electrocatalyst, suggesting that O_2 is the primary product of water oxidation in this case.[35]

Since the nickel center of the Ni(II)TCPP linkers serves as the active catalytic site within the MOF, the mechanism for water oxidation by PCN-224-Ni is expected to proceed *via* similar reaction steps to that of a homogeneous Ni(II) porphyrin in solution. Due to the rigid nature of the PCN-224-Ni MOF and the fact that the distances between Ni(II)-centers within the framework are ~19 Å between co-facial porphyrins lining the same channel and ~14 Å between orthogonal porphyrins (Fig. S1†), it is unlikely that the catalytic mechanism involves interactions between neighboring Ni(II) porphyrins. It has been proposed previously by Han *et al.* for a cationic, water soluble Ni(II) tetrakis(4-*N*-methylpyridyl)porphyrin molecular catalyst that the first step of the catalytic cycle is the oxidation of the porphyrin to generate the radical cation species, Por$^{•+}$–Ni(II).[35] This mechanistic step is supported by the Tafel analysis, which suggests that an electrochemical reaction occurs as the necessary first step. The porphyrin oxidation is followed by binding of a water molecule to the Ni(II) metal center (Scheme 1) to generate Por$^{•+}$–Ni(II)–OH$_2$. Sequential proton and electron transfer reactions result in the deprotonation of the coordinated water molecule with concomitant oxidation of the Ni(II) center to give the hydroxide bound species, Por$^{•+}$–Ni(III)–OH. The intramolecular electron transfer from the hydroxide to the porphyrin ring coupled with the abstraction of a proton gives rise to Por–Ni(III)–O$^•$. Following the O–O bond formation step, the peroxide bound species, Por–Ni(II)–OOH, is generated, which undergoes another proton-coupled electron transfer reaction to give Por–Ni(II)–OO$^•$. The final oxidation process results in the release of O_2 and the regeneration of the starting Por–Ni(II) complex.[35]

Proton management is required for catalysts to operate at neutral pH.[47] At pH 7, water is a very weak base and present at too low of a concentration (1×10^{-7} M) to effectively fill the role of proton acceptor. In this sense, the mechanism of PCN-224-Ni and the homogeneous catalyst differ dramatically. Computational modeling of the homogeneous catalyst performed by Han *et al.* indicated that the O–O bond formation and subsequent deprotonation proceeds *via* a low energy route when mediated by an added molecular base, such as phosphate or acetate. Both of these weak bases are incompatible with the PCN-224-Ni framework. However, with the Ni(II) porphyrin situated inside the framework another possibility presents itself. It was recently reported by Hupp *et al.* that Zr–oxo nodes in related PCN and UiO MOFs could act as proton acceptors, particularly coordinated water (Zr–OH$_2$) and hydroxyl (Zr–OH) species for which pK_a values were measured in 5.71–6.80 and 8.11–8.32 ranges, respectively.[48] Therefore, we propose that the Zr–oxo nodes serve as the proton acceptors in a cooperative fashion with the linker catalyst, providing a new class of secondary proton management possibilities. The distance between the water molecule on the Ni center and Zr–oxo cluster is 10.7 Å (Fig. S9†), which means that three water molecules would be required to form a continuous H-bonded network capable of facilitating proton transport. To our knowledge, this is the first example of cooperative linker–node interactions that promote chemistry not possible under different constructs. The coordinated water (Zr–OH$_2$) and hydroxyl (Zr–OH) groups typically originate at missing-linker defect sites,[49] however, Zr–oxo clusters inside PCN-224-Ni already contain 6 terminal oxygen atoms, each of which could potentially accept protons from the water oxidation reaction. The number of available Zr–oxo nodes present in the framework is limited (node : linker ratio is 2 : 3) and is only sufficient to complete one electrochemical cycle, assuming that each node can accept 6 protons and each linker generates 4 protons per cycle. This limitation would account for the low TON observed (0.72) during the electrolysis experiment. It is also possible that Zr–oxo clusters merely serve as conduits and the proton is transferred to the bulk water. The exact role of the nodes in the electrochemical oxidation of water by Ni(II)TCPP remains elusive and studies are underway to gain deeper insights into the nature of proton transfer in this MOF. That said, the prospect of cooperative behavior between redox-active linkers and Brønsted basic SBUs could lead to the development of novel MOF-based electrocatalysts.

Thorough stability investigations are crucial in establishing that the MOF is indeed an active electrocatalytic species and not merely acting as a precursor for its formation, as metal ions often undergo considerable rearrangements of their coordination spheres during the redox cycling. This has been demonstrated in the Co-based ZIF-67, which is comprised of redox-active metal nodes that underwent irreversible decomposition upon anodic potentials.[50] Therefore, certain porphyrin-containing frameworks, such as [Pb$_2$(H$_2$TCPP)]·4DMF·H$_2$O, despite showing electrocatalytic activity towards water oxidation, are less likely to retain their structure during the electrolysis.[31] To the best of our knowledge, only 3 examples of intrinsic MOF water oxidation electrocatalysts were reported in the literature to date.[31–33] Within these reports, however, extensive characterization of the framework pre- and post-electrolysis is lacking. In the case of nickel-based systems,
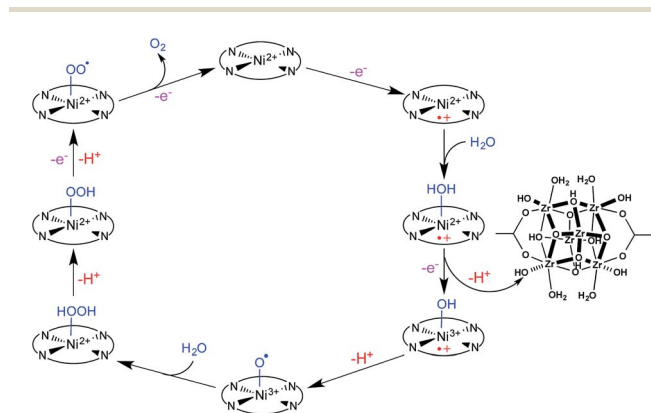
Scheme 1 Proposed mechanism for the electrochemical water oxidation reaction catalyzed by PCN-224-Ni.[35] Some carboxylate groups have been omitted from the Zr node for clarity.

This journal is © The Royal Society of Chemistry 2016

J. Mater. Chem. A, 2016, **4**, 16818–16823 | **16821**

electrocatalytically-active oxide and hydroxide films have been formed from soluble nickel complexes at the oxidative potentials used for water oxidation experiments.[51,52] As a result, the present work provides a detailed characterization of the MOF and demonstrates the stability of the PCN-224-Ni films towards electrolysis conditions using several characterization techniques.

X-ray photoelectron spectroscopy (XPS) of the MOF film revealed that the position and the shape of Ni 2p and N 1s signals remained largely unchanged before and after electrolysis (Fig. S10A and B†), indicating that the Ni(II)TCPP core did not experience any significant coordination geometry rearrangements and/or redox state changes. In addition, SEM images (Fig. S10C and D†) showed that MOF particles retained their size and morphology, suggesting that they did not undergo any solid–solid transformations or dissolution. Further analysis on digested PCN-224-Ni films after electrolysis *via* ICP found the Zr : Ni ratio to be 4.71 : 1, which is comparable to the ratio found in the as-synthesized framework (the theoretical Zr : Ni ratio should be 4 : 1 based on the molecular formula of PCN-224-Ni, $C_{144}H_{72}N_{12}O_{64}Ni_3Zr_{12}$).[20] These results suggest that the MOF remaining on FTO after electrolysis is indeed PCN-224-Ni. Additionally, the amounts of Ni and Zr detected in solution post-electrolysis represent 7.2% and 1.8% of the total contents of the MOF films, respectively (Table S1†). This result could be attributed to the detachment of mechanically-bound MOF particles from FTO substrate into solution.

To summarize, the Zr(IV)-based MOF with Ni(II)TCPP linkers, PCN-224-Ni, was grown solvothermally onto conductive FTO substrates and shown to electrochemically oxidize water. The mechanism of water oxidation was found to be best described by a rate-determining electrochemical step followed by a chemical reaction with Ni(II)TCPP playing the role of the active catalytic sites and Zr nodes acting as proton abstractors. The work brings to light the ability to promote unique reactivity within MOFs through the dual design of both the linker and node. The structure of the PCN-224-Ni was found to remain intact during the electrochemical reaction. As such, incorporation of active molecular catalysts into highly robust Zr-based scaffolds can be used as a viable strategy for the design of electrocatalytic frameworks. Application of MOFs in the electrocatalytic oxidation of water is still in its early stages with a lot of room for improvements in catalyst design and this study serves as an important milestone towards better understanding of these systems.

Acknowledgements

Notes and references

1 N. S. Lewis, *Chem. Rev.*, 2015, **115**, 12631–12632.
2 N. S. Lewis and D. G. Nocera, *Proc. Natl. Acad. Sci. U. S. A.*, 2006, **103**, 15729–15735.
3 C. H. Lee, D. K. Dogutan and D. G. Nocera, *J. Am. Chem. Soc.*, 2011, **133**, 8775–8777.
4 C. Costentin, S. Drouet, M. Robert and J.-M. Savéant, *Science*, 2012, **338**, 90–94.
5 D. L. DuBois, *Inorg. Chem.*, 2014, **53**, 3935–3960.
6 J. W. Raebiger, J. W. Turner, B. C. Noll, C. J. Curtis, A. Miedaner, B. Cox and D. L. DuBois, *Organometallics*, 2006, **25**, 3345–3351.
7 Y. Zhao, J. R. Swierk, J. D. Megiatto Jr, B. Sherman, W. J. Youngblood, D. Qin, D. M. Lentz, A. L. Moore, T. A. Moore, D. Gust and T. E. Mallouk, *Proc. Natl. Acad. Sci. U. S. A.*, 2012, **109**, 15612–15616.
8 M. Eddaoudi, J. Kim, N. Rosi, D. Vodak, J. Wachter, M. O'Keeffe and O. M. Yaghi, *Science*, 2002, **295**, 469–472.
9 D. Farrusseng, S. Aguado and C. Pinel, *Angew. Chem., Int. Ed.*, 2009, **48**, 7502–7513.
10 J. Y. Lee, O. K. Farha, J. Roberts, K. A. Scheidt, S. B. T. Nguyen and J. T. Hupp, *Chem. Soc. Rev.*, 2009, **38**, 1450–1459.
11 Q. Z. Zha, X. Rui, T. T. Wei and Y. S. Xie, *CrystEngComm*, 2014, **16**, 7371–7384.
12 W. Y. Gao, M. Chrzanowski and S. Q. Ma, *Chem. Soc. Rev.*, 2014, **43**, 5841–5866.
13 Q. Zha, X. Rui, T. Wei and Y. Xie, *CrystEngComm*, 2014, **16**, 7371–7384.
14 Z. Guo and B. Chen, *Dalton Trans.*, 2015, **44**, 14574–14583.
15 I. Bhugun, D. Lexa and J.-M. Saveant, *J. Am. Chem. Soc.*, 1996, **118**, 1769–1776.
16 M. W. Grinstaff, M. G. Hill, J. A. Labinger and H. B. Gray, *Science*, 1994, **264**, 1311–1313.
17 K. Kadish, R. Guilard and K. Smith, *The Porphyrin Handbook*, Academic Press, 2003.
18 I. Hod, M. D. Sampson, P. Deria, C. P. Kubiak, O. K. Farha and J. T. Hupp, *ACS Catal.*, 2015, **5**, 6302–6309.
19 D. Feng, Z. Y. Gu, J. R. Li, H. L. Jiang, Z. Wei and H. C. Zhou, *Angew. Chem.*, 2012, **124**, 10453–10456.
20 D. Feng, W.-C. Chung, Z. Wei, Z.-Y. Gu, H.-L. Jiang, Y.-P. Chen, D. J. Darensbourg and H.-C. Zhou, *J. Am. Chem. Soc.*, 2013, **135**, 17105–17110.
21 B. J. Deibert and J. Li, *Chem. Commun.*, 2014, **50**, 9636–9639.
22 J. Zheng, M. Wu, F. Jiang, W. Su and M. Hong, *Chem. Sci.*, 2015, **6**, 3466–3470.
23 A. Fateeva, P. A. Chater, C. P. Ireland, A. A. Tahir, Y. Z. Khimyak, P. V. Wiper, J. R. Darwent and M. J. Rosseinsky, *Angew. Chem.*, 2012, **124**, 7558–7562.
24 D. Feng, Z.-Y. Gu, Y.-P. Chen, J. Park, Z. Wei, Y. Sun, M. Bosch, S. Yuan and H.-C. Zhou, *J. Am. Chem. Soc.*, 2014, **136**, 17714–17717.
25 W. Morris, B. Volosskiy, S. Demir, F. Gándara, P. L. McGrier, H. Furukawa, D. Cascio, J. F. Stoddart and O. M. Yaghi, *Inorg. Chem.*, 2012, **51**, 6443–6445.
26 S. Yuan, T.-F. Liu, D. Feng, J. Tian, K. Wang, J. Qin, Q. Zhang, Y.-P. Chen, M. Bosch, L. Zou, S. J. Teat, S. J. Dalgarno and H.-C. Zhou, *Chem. Sci.*, 2015, **6**, 3926–3930.
27 N. Kornienko, Y. Zhao, C. S. Kley, C. Zhu, D. Kim, S. Lin, C. J. Chang, O. M. Yaghi and P. Yang, *J. Am. Chem. Soc.*, 2015, **137**, 14129–14135.

16822 | *J. Mater. Chem. A*, 2016, **4**, 16818–16823

This journal is © The Royal Society of Chemistry 2016

28 A. Herbst, A. Khutia and C. Janiak, *Inorg. Chem.*, 2014, **53**, 7319–7333.

29 M. Lammert, M. T. Wharmby, S. Smolders, B. Bueken, A. Lieb, K. A. Lomachenko, D. D. Vos and N. Stock, *Chem. Commun.*, 2015, **51**, 12578–12581.

30 F. Vermoortele, B. Bueken, G. Le Bars, B. Van de Voorde, M. Vandichel, K. Houthoofd, A. Vimont, M. Daturi, M. Waroquier, V. Van Speybroeck, C. Kirschhock and D. E. De Vos, *J. Am. Chem. Soc.*, 2013, **135**, 11465–11468.

31 F. Dai, W. Fan, J. Bi, P. Jiang, D. Liu, X. Zhang, H. Lin, C. Gong, R. Wang, L. Zhang and D. Sun, *Dalton Trans.*, 2016, **45**, 61–65.

32 S. Wang, Y. Hou, S. Lin and X. Wang, *Nanoscale*, 2014, **6**, 9930–9934.

33 E. A. Flügel, V. W. H. Lau, H. Schlomberg, R. Glaum and B. V. Lotsch, *Chem.–Eur. J.*, 2016, **22**, 3676–3680.

34 D. Chang, T. Malinski, A. Ulman and K. M. Kadish, *Inorg. Chem.*, 1984, **23**, 817–824.

35 Y. Z. Han, Y. Z. Wu, W. Z. Lai and R. Cao, *Inorg. Chem.*, 2015, **54**, 5604–5613.

36 K. Kalyanasundaram and M. Neumannspallart, *J. Phys. Chem.*, 1982, **86**, 5163–5169.

37 M. W. Renner and J. Fajer, *JBIC, J. Biol. Inorg. Chem.*, 2001, **6**, 823–830.

38 S. Dey, B. Mondal and A. Dey, *Phys. Chem. Chem. Phys.*, 2014, **16**, 12221–12227.

39 A. J. Esswein, Y. Surendranath, S. Y. Reece and D. G. Nocera, *Energy Environ. Sci.*, 2011, **4**, 499–504.

40 R. D. L. Smith, M. S. Prévot, R. D. Fagan, S. Trudel and C. P. Berlinguette, *J. Am. Chem. Soc.*, 2013, **135**, 11580–11586.

41 Y. Surendranath, D. K. Bediako and D. G. Nocera, *Proc. Natl. Acad. Sci. U. S. A.*, 2012, **109**, 15617–15621.

42 Y. Surendranath, M. W. Kanan and D. G. Nocera, *J. Am. Chem. Soc.*, 2010, **132**, 16501–16509.

43 S. Fletcher, *J. Solid State Electrochem.*, 2009, **13**, 537–549.

44 E. Gileadi, *Electrode Kinetics for Chemists, Engineers, and Materials Scientists*, VCH Publishers, Inc., New York, 1993.

45 S. R. Ahrenholtz, C. C. Epley and A. J. Morris, *J. Am. Chem. Soc.*, 2014, **136**, 2464–2472.

46 D. L. DuBois, A. Miedaner and R. C. Haltiwanger, *J. Am. Chem. Soc.*, 1991, **113**, 8753–8764.

47 M. W. Kanan and D. G. Nocera, *Science*, 2008, **321**, 1072–1075.

48 R. C. Klet, Y. Liu, T. C. Wang, J. T. Hupp and O. K. Farha, *J. Mater. Chem. A*, 2016, **4**, 1479–1485.

49 C. A. Trickett, K. J. Gagnon, S. Lee, F. Gándara, H.-B. Bürgi and O. M. Yaghi, *Angew. Chem.*, 2015, **127**, 11314–11319.

50 P. M. Usov, C. McDonnell-Worth, F. Zhou, D. R. MacFarlane and D. M. D'Alessandro, *Electrochim. Acta*, 2015, **153**, 433–438.

51 A. Singh, S. L. Chang, R. K. Hocking, U. Bach and L. Spiccia, *Catal. Sci. Technol.*, 2013, **3**, 1725–1732.

52 A. Singh, S. L. Y. Chang, R. K. Hocking, U. Bach and L. Spiccia, *Energy Environ. Sci.*, 2013, **6**, 579–586.